PRACA ORYGINALNA

Received: 20.06.2014
Revised: 25.08.2014
Accepted: 08.09.2014
Published online: 12.11.2014

Applying Data Mining and Machine Learning Algorithms to predict symptom development in Parkinson's disease

Stosowanie eksploracji danych i algorytmów uczenia maszynowego do przewidywania rozwoju objawów w chorobie Parkinsona

Andrzej W. Przybyszewski

University of Massachusetts Medical School, Department Neurology, 65 Lake Av., Worcester, MA 01655, USA
Polish-Japanese Institute of Information Technology, Koszykowa 86, 02-008 Warszawa, Poland

ABSTRACT

The standard treatment of PD symptoms depends on the experience of a particular neurologist, UPDRS and Hoehn and Yahr scale measurements in order to estimate the stage of PD, the patient's reports and patient's responses to medications. All these estimations are to a great extent subjective and determine different treatments in different centers. The purpose of this work was to develop an approach that may more precisely and objectively estimate a patient's symptoms and in consequence optimize individual PD treatment. We have presented several examples of different methods that make measurements in PD more precise. However, greater precision and objectivity were only the first steps. In addition, all (standard and new) data must be evaluated in an intelligible way in order to better estimate PD symptoms and their developments. We have used data mining and machine learning approaches to mimic the "golden" neurologist's reasoning.

KEY WORDS
data mining, machine learning algorithms, Parkinson's disease

STRESZCZENIE

Standardowe leczenie objawów PD zależy od doświadczenia danego neurologa oraz wyników pomiarów w skalach UPDRS oraz Hoehn i Yahr, aby ocenić stadium choroby Parkinsona, opinii pacjenta i jego reakcji na leki. Wszystkie oceny stosowane w tym celu są w dużej mierze subiektywne. Celem niniejszej pracy było opracowanie podejścia, które mogłoby bardziej precyzyjnie i obiektywnie oszacować fluktację objawów pacjenta i w konsekwencji optymalizację indywidualnego traktowania PD. Pokazaliśmy kilka przykładów różnych metod, które zwiększają precyzję pomiarów w PD. Trzeba zaznaczyć, że większa precyzja i obiektywność są tylko pierwszym krokiem. Ostatecznie wszystkie dane (otrzymane zarówno nowymi, jak i standardowymi metodami) muszą być po-

ADRES DO KORESPONDENCJI:

Prof. dr hab. Andrzej W. Przybyszewski
Polish-Japanese Institute
of Information Technology
ul. Koszykowa 86
02-008 Warszawa
tel: +48 22 58 44 500; fax: +48 22 58 44 501
e-mail: Andrzej.Przybyszewski@umassmed.edu

Ann. Acad. Med. Siles. 2014, 68, 5, 332–349

eISSN 1734-025X
www.annales.sum.edu.pl

równane w czytelny sposób, aby lepiej ocenić nasilenie i rozwój objawów PD. Użyta metoda eksploracji danych i algorytm uczenia maszynowego mają naśladować „złoty" tok rozumowania neurologa.

SŁOWA KLUCZOWE
eksploracja danych, algorytmy uczenia, choroba Parkinsona

INTRODUCTION

The most popular approach to study symptom developments in Parkinson's disease (PD) patients is to use statistical methods. By applying statistics to large databases, one can find significant information about the specificity of PD. As larger databases have information from different PD clinics, one can compare the results of different treatments. Nevertheless, due to the various types of care, some of the results obtained even from the most prominent expert centers might be inconsistent. Applying statistical averaging methods to such inconsistences may give confusing results even leading to statements that a specific type of care does not effectively influence PD patients.

We might face similar problems when explaining factors that result in longer, better, and more active lives of people with Parkinson's. Generally we agree that controlling depression and movement therapies is the main factor in helping patients. However, different clinics use different methods in dealing with depression. They also may interpret differently meanings of the UPDRS that results in different therapies. These problems are articulated in the popular statement "*No two people face Parkinson's in quite the same way."* People vary substantially in their combination of symptoms, rate of progression, and reaction to treatment. Again, averaging patients' symptoms as the effects of different types of care gives a very crude approximation of the results. If we would like to improve this analysis, we need to take into account a great variety of patient symptoms and inconsistent effects of care in different PD clinics.

Therefore, we propose to extend the statistical analysis by **data mining and machine learning (ML) methods** which give a higher meaning to an individual patient's symptoms and their individual developments. In consequence, our methods will suggest a specific treatment adjusted to different individual patients that may lead to slowing down their symptoms and improving their quality of life. These treatments will be proposed on the basis of **learning algorithms** that intelligently process the data of the individual patient in a specific way. Our method of symptom classification will be similar to complex object recognition by a visual system. The ability of the visual system to recognize various objects arises in the afferent, ascending pathways that classify the properties of object parts from simple attributes in lower areas, to more complex ones in higher areas. These primary classifications are compared and adjusted by interaction with all the object ("holistic") properties (representing visual knowledge) on all levels by descending pathway influences [1]. These interactions on multiple levels between measurements and knowledge with the help of learning can differentiate subtle variations in symptoms and treatments similar to studying complex visual objects [2,3]. By using predictions with the support of machine learning algorithms, we will discover if these subtle variations are significant enough to improve the patient's treatment.

The popular statement that "*No two people face Parkinson's in quite the same way"* may describe the Parkinson's patient's point of view on his/her disease. The patient's self perception is subjective and depends on many factors but mostly on emotional states that are often related to depression and motor impairments. Social support or its lack is also an important factor. Furthermore, the opinions of neurologists who follow a patient's symptoms are important for the patient. However, the opinion of the neurologist is more objective as supported by objective but mostly not very precise interviews, tests and measurements of the patient's symptoms like e.g. UPDRS. Other views on the patient's state come from psychologists, caregivers or family members. All these opinions describing the patient's actual status are often not consistent and sometimes even contradictory especially if the patient's conditions fluctuate with medications and the time of day or night. To make things even more complicated, there is strong dependence between different symptoms, for example, a caregiver can perform exercises with a patient that make the patient feel good, but in reality may not improve the patient's motor skills.

There are many well-established patient symptom measures such as the most common Hoehn and Yahr scale and total UPDRS. However, even if non-motor symptoms and motor complications are common in PD, UPDRS Parts I and IV that focus on non-motor symptoms are used infrequently. In most "PubMed" publications between 1998–2011, in all the studies that have used UPDRS, 163 studies (97.6%) had included only UPDRS part III [4]. There are many different measures of PD symptoms describing actual patient state and their values mostly, like UPDRS, increase with time and disease progression. As there is actually no cure that can stop Parkinson's disease development, there are only some possibilities to slow

it down. The main purpose of this paper is to analyze such means by using knowledge extracted from the symptoms.

We will demonstrate our approach using several examples of patients with DBS (deep brain stimulation) therapy which is mostly used in more advanced PD stages. In order to be effective, stimulating electrodes must be placed precisely in or near the STN (subthalamic nucleus). As the STN is in most cases invisible in the MRI, the standard procedure is related to the intra-OP neuronal activity recording that helps in verifying that the microelectrode tip is in/near the STN. As it is not a straight-forward task, and we have described (see below) how to increase and automatize this procedure using several different approaches: by looking at changes in the power spectra of the high and low (local field potentials – LFP) frequency background activity, or by using different algorithms to find properties of the spike train related to the STN. We have also discussed methods of finding the exact position of the stimulating electrode in relationship to the STN. What effects can be expected by stimulation of the specific contact of the DBS electrode as a function of its relationship to different STN parts? The central and peripheral effects related to the DBS electrode position can be estimated and precisely measured in different effectors. On the one hand, we have described correlations between UPDRS and Euler hip angle changes of the gait. On another central side, we have measured the correlation between UPDRS and eye movement pathologies. All these various measurements might help in more precise estimation and control of PD symptom development and in consequence improve patient care.

METHODS

Let us assume that the complex shape in Fig. 1 represents the set of different symptoms. Our methods can measure of symptom values with a certain precision represented by squares (granules). Therefore, on the basis of our measurements we can get two approximations of the patient's real symptoms: the **lower approximation** set as squares inside the curve (Fig. 1 black squares) and the **upper approximation** set is represented by squares that cover the whole shape (gray and black squares). The lower approximation set represents all the actual symptoms (values) that are certain, whereas the upper approximation set represents symptoms (values) that are not all certain. The white squares represent symptoms that are not present in the patient. The set between the upper and lower approximations represent the border region (gray squares). This region represents symptoms that fluctuate in time or symptoms that cannot be exactly determined or measured by the neurologist. We can normalize the symptom values in a similar way as UPDRS values (0–4). In this case, if there is no pathology/symptoms or movements are normal, all the values are 0. Therefore for a normal person, the shape-describing the symptoms consist only of a point.

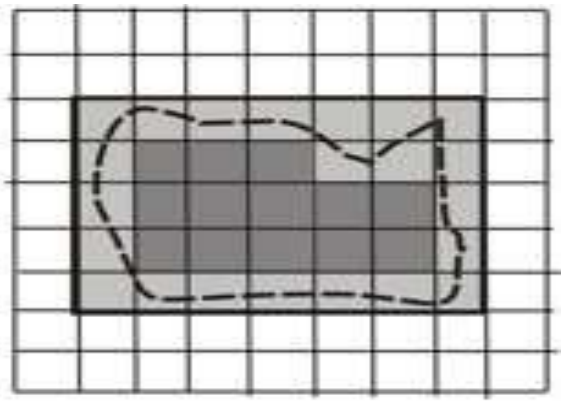

Fig. 1. Diagram showing possible set roughness in symptom classification.
Ryc. 1. Schemat obrazujący możliwy zbiór niepewności w klasyfikacji objawów.

In this model, different patients may have shapes with different complexities. The progression of the disease when symptoms become more severe correlates with shape expansion. It expands differently in different patients but the area always increases as the symptom values become larger. We would like to find in which direction the expansion is the fastest and try to slow it down. However, we still have several issues with this simple model. At first, the symptoms are not independent so that the fastest expansion may cause or may be caused by a change in other symptoms. The sensitivity of our measurements is limited, so we do not sense symptom changes in the border region, etc. Also another problem is related to the different weights of symptoms, for example, the danger of falling is more important than a slow or asymmetric walk. There is a subjective, patient's point of view, nevertheless, the doctor's role is to find which symptoms are the most important to follow. Neurologists get this knowledge from their experience, but we would like to extract this knowledge from the database. Our data mining methods can tell us which measurements are important for our classifications. However, in general, in order to find which symptom has the fastest growth, we need to interview and observe patients. An experienced neurologist can find such differences even if the total UPDRS does not change significantly. Nonetheless, even in the best clinics, experienced neurologists have limited time and cannot follow every patient all the time in order to perform more precise measurements. The long-term purpose of our approach is to propose a solution to these problems.

1. Theoretical Basis

The data structure is an important point of our analysis. It is represented in the form of an information system or decision table. We define after [5] an information system as $S = (U, A)$, where U, A are nonempty finite sets called the *universe of objects* and the *set of attributes*, respectively. If $a \in A$ *and* $u \in U$, value $a(u)$ is a unique element of V (where V is a value set).
We define the **lower approximation** of symptoms set $X \subseteq U$ in relation to symptom attribute B as $\underline{B}X = \{u \in U: \lceil u]_B \subseteq X\}$, and the **upper approximation** of X as $\overline{B}X = \{u \in U: [u]_B \cap X \neq \phi\}$. In other words, all the symptoms are classified into two categories (sets). The lower approximation set has a property that all symptoms with certain attributes that are a part of set X, and the upper movement approximation set has a property that only some symptoms with B attributes are a part of X (for more details see [5]). The difference between $\overline{B}X$ *and* $\underline{B}X$ is defined as the boundary region of X: $BN_B(X)$. If $BN_B(X)$ is an empty set, then X is *exact* (*crisp*) with respect to B; otherwise if $BN_B(X) \neq \phi$ and X is not *exact* (i.e., it is *rough*) with respect to B. We say that the B-lower approximation of a given set X is the unified set of all *B-granules* that are included in set X, and the B-upper approximation of X is of the union of all *B-granules* that have a nonempty intersection with X. System S will be called decision table $S = (U, C, D)$ where ***C* is the condition** and ***D* is the decision attribute** [5]. In the table below (tab. I), as an example, decision attribute D, based on expert opinion, is placed in the last column, and the condition attributes measured by a neurologist, are placed in other columns. **On the basis of each row in the table, the rules describing the symptoms of each patient can be proposed.** As you can see, these rules have many particular conditions. The main concept of our approach is to describe different symptoms in different patients by using such rules. On the basis of these rules, using the **modus ponens rule,** we want to find universal rules for different symptoms and different patients.
However, the symptoms, even for the same treatments are not always the same; therefore our rules must have certain "flexibility", or granularity, which can be interpreted as the probability of finding certain symptoms in a group of patients under consideration.
The granular computation simulates a way in which neurologists interact with patients. This way of thinking relies on the ability to perceive a patient's symptoms under various levels of granularity (i.e., abstraction) in order to extract and consider only those things that serve a specific interest and to switch among different granularities. By focusing on different levels of granularity, one can obtain different levels of knowledge, as well as greater understanding of the inherent knowledge structure. Granular computing is thus essential in human-like, intelligent problem solving behaviors in *problem-specific* tasks.
The ***indiscernibility relation*** of any subset B of A or $I(B)$, is defined [5] as follows: $(x, y) \in I(B)$ or $xI(B)y$ if and only if $a(x) = a(y)$ for every $a \in B$, where $a(x) \in V$. $I(B)$ is an equivalence relation, and $[u]_B$ is the equivalence class of u, or a *B-elementary granule*. The family of all the equivalence classes of $I(B)$ will be denoted as $U/I(B)$ or U/B. The block of partition U/B containing u will be denoted by $B(u)$. Having the discernibility relation, we define the notion of reduct $B \subset A$ as a reduct of the information system if $IND(B) = IND(A)$ and no proper subset of B has this property. In the case of a decision tables decision, the **reduct is set $B \subset A$ of attributes such that it cannot be further reduced** and IND(B) $\subset$ IND(d). The decision rule is a formula of the form $(a_{i1} = v_1) \wedge ... \wedge (a_{ik} = v_k) \Rightarrow d = v_d$, where $1 \leq i_1 < ... < i_k \leq m$, $v_i \in Va_i$. Atomic subformulas $(a_{i1} = v_1)$ are called conditions. We say that rule r is applicable to an object, or alternatively, the object matches the rule, if its attribute values satisfy the rule. With the rule we can connect some numerical characteristics such as matching and support.
In order to **replace original attribute a_i with a new, binary attribute** which says whether an actual attribute value for an object is greater or lower than c (more in [6]), we define c as a cut ***(cut sets)***. As cut for attribute $a_i \in A$, such that Va_i is an ordered set, we will denote the value $c \in Va_i$. The template of A is a propositional formula: $v_i \in Va_i$. A generalized template is the formula of the form $\wedge(a_i \in T_i)$ where $T_i \subset Va_i$. An object satisfies (matches) a template if for every attribute a_i $(a_i = v_i)$ where $a_i \in$ A. The template is a natural way to split the original information system into two distinct sub-tables. One of those sub-tables consists of objects that satisfy the template, the second one of all the others. **A decomposition tree** is defined as a binary tree, whose every internal node is labeled by a template, and an external node (leaf) is associated with a set of objects matching all the templates in a path from the root to a given leaf [6]. We use the decomposition tree in ML algorithms.

2. Intraoperative Recordings

I will describe in short the surgery performed at UMass Medical School as described in detail in [7]. Similar surgeries were performed by Dr. Kwiek in MUS [8,9] and Dr. Mandat [10] in the Institute of Psychiatry and Neurology (Warsaw). Surgical planning at UMass utilized BrainLab iPlan Stereotaxy 2.6 (BrainLAB AG, Germany), which allows for multiplanar imaging of the target and the planned trajectory(s). T2 weighted and enhanced T1 MRI sequences

were acquired pre-operatively. In relationship to the midcommisural (AC-PC) point, the target is expected to be 11–12 mm lateral, 3 mm posterior and 4 mm below**.** According to the anatomy atlas, the usual trajectory penetrated the following structures: anterior thalamus, zona incerta, H2 field of Forel, STN, and substantia nigra (SN).

All the electrophysiological recordings were performed at UMass using a Guideline 4000 (FHC, Inc. Bowdoin, ME). The neural signals were recorded by one or more parallel tungsten microelectrodes. The recordings started 20 or 10 mm above the target (different centers). The microelectrode(s) was (were) advanced at 1 to 0.3 mm increments. Ten second recordings were obtained at each point. The recordings were band-pass filtered in two frequency ranges: high frequency (300–5000 Hz), digitized at 24 kHz related to the spike trains and low frequency range (5––500 Hz) with a sampling rate of 1000Hz related to the local field potentials and stored for offline analysis [7].

The electrophysiological criteria used by neurologists to distinguish the STN were an increase in the background activity, an increase in the neuronal firing, and/or alteration of neural firing by passive movement of contralateral limbs**.** The entry to the STN corresponds to the dorsal border and the exit from the STN to the ventral border.

Off-line analyses were performed with software written in Matlab (Matworks, Natick, MA). STN detection is based on the MUA profile (multi-unit activity) which is characteristically elevated within the STN. Large spikes were automatically removed by an unsupervised Daubechies-based wavelet algorithm that is a spike-oriented modification of the standard wavelet-denoising algorithm with soft-thresholding [7]. The MUA was calculated in the frequency domain. The power spectral density was calculated over 10-second segments of despiked neuronal activity or LFP with a Fourier transform (FFT) weighted by a Hamming window. The MUA was obtained by integrating the 500–2000 Hz band in the power spectral density (psd) [7]. The LFP was obtained by integrating the 20––35 Hz band in psd.

The dorsal STN border was defined as the first site along a track where the MUA exceeds the MUA baseline by at least 50% and elevation of the MUA is sustained. The baseline MUA was obtained as an average MUA from recordings ≥ 10 mm above the target that usually correspond to thalamic activity. The ventral border was defined as the last site along a track where the MUA reduction was 50% compared to the average MUA within the STN and the decline in MUA is sustained [7]. Similar criteria were used for the LFP.

3. DTI/MRI registration to anatomical atlas

In this section, we describe how to define the relationship between the electrode' position and STN borders. In short, in order to determine the anatomical positions of the structures of interest, we performed registration of the individual patient's brain MRIs with the brain atlas and used postoperative MRI or CT to locate the exact position of the implanted DBS electrodes [11]. In addition, in order to find which part of the cortex might be stimulated by different contacts, we used preoperative diffusion weighted images (DWI) acquired as part of the standard procedure for each PD patient. However, one extra condition must be fullfilled in order to get highly precise measurements, MRI data has to have a small slice thickness and equal spacing in all directions. We analyzed data from nine patients with advanced Parkinson disease (PD), and with implanted DBS electrodes. As the image processing tool we used the 3D Slicer (Harvard Medical School) public domain software. As in the postoperative images the electrode contacts can are not visible, we estimated their positions by using the physical parameters of the used stimulating electrodes (Medtronic 3389) [12]. In order to estimate the traced areas, coordinates of the brain have to be normalized by a so-called AC-PC transform (3D Slicer). The connections between M1, SMA and STN have somatotopic properties that gave us the basis to estimate the expected motor effects related to the stimulation of different contacts [13,14].

4. MoCap (Motion Capture) method

In our kinematic movement recording set-up, we used a 10-camera, 3D motion capture system (MoCap--Vicon) as described in [16]. The 3D body position of the patient was analyzed based on 39 reflective markers (tracked at 100 FPS) placed on major body segments: 4 on the head, 5 on the torso, 14 on the left and right side of the upper limbs and 16 on the left and right side of the lower body. Two Kistler Platforms were also recorded to analyse the Ground Reaction Forces (GRF) during the patient's movements, but we will not present GRF data in this paper (Fig. 1) [15].

We performed experiments on 12 Parkinson Disease (PD) patients who have undergone surgery in the Dept. of Neurosurgery, Medical University of Silesia (MUS, Poland) in order to implant a Deep Brain Stimulator (DBS) to improve their motor skills. The patients were qualified for surgery and observed postoperatively in the MUS Dept. of Neurology [9,10]. All the experiments were performed in the MoCap lab of PJIIT in Bytom (Polish-Japanese Institute of Infor-

mation Technology, Bytom, Poland). The PD patients performed normal walking under four experimental conditions (S1–S4 – see below) defined by pharmacological medication and subthalamic nucleus (STN) electrical stimulation (DBS).

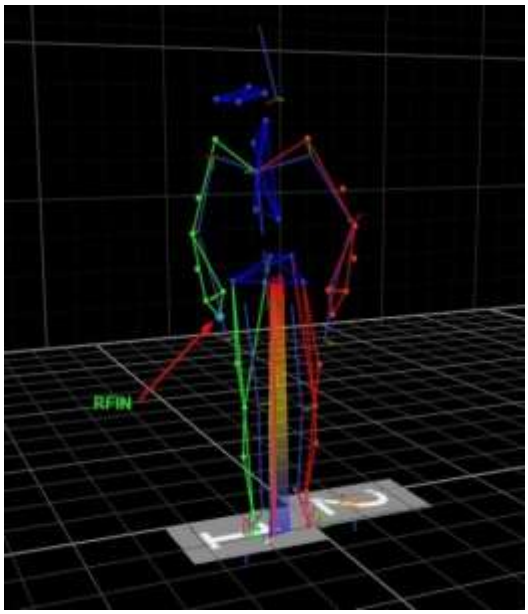

Fig. 2. MoCap set-up.
Ryc. 2. Konfiguracja Mo-Cap.

5. Eye movement measurements

The characteristic motor symptoms of PD, predominantly due to progressive degeneration of nigral dopaminergic neurons, are initially subtle and impact purposeful movement, and are often difficult to diagnose and differentiate from other age related symptoms. An easy and objective method to measure PD patient symptoms is by testing the patient's eye movements.

We conducted horizontal RS (reflexive saccades) measurements in nine patients with Parkinson's disease (PD) in four sessions: S1: MedOffDBSOff, S2: MedOffDBSOn, S3: MedOnDBSOff, S4: MedOnDBSOn. Changes in motor performance, behavioral dysfunction, cognitive impairment and functional disability were evaluated in each session according to the UPDRS. RS were recorded by a head-mounted saccadometer (Ober Consulting, Poland).

We used the infrared eye track system coupled with the head tracking system (JAZZ-pursuit – Ober Consulting, Poland) in order to get high accuracy and precision in eye tracking in order to compensate the possible subject's head movements relative to the monitor. Therefore, the subjects do not have to be positioned in an unnatural chinrest. A patient was sat at the distance of 60–70 cm from the monitor with his head supported by the chair in order to minimize head movements. We measured the fast eye movements in response to a spot of light switching off-on and moving horizontally from the straight eye fixation position (0 deg) to 15 deg to the left or 15 deg to the right after an arbitrary period of time: 0.5–1.5 s. When the patient fixates his/her eyes on the spot of the middle marker (0 deg), the spot will change color: from white to green, which means that the patient should perform RS (reflexive saccades); or from white to red meaning to perform AS (antisaccades). Then the central spot will be switched off and one of the two peripheral targets, selected at random with equal probability, will be illuminated instead. The patient has to look at the targets and follow them as they move in the RS task or make opposite direction saccades in the AS task. After making a saccade to the peripheral target, the target will remain on for 0.1 s and then another trial will begin. In each test the subject had to perform 20 RS and 20 AS in a row in Med-off in two situations: with DBS off (S1) and DBS on (S2). In the next step, the patient took medication and had a break for a half to one hour, then the subject performed the same experiments with DBS off (S3) and DBS on (S4). In this work, we have analyzed only RS data using the following population parameters averaged for both eyes: delay mean ± SD; amplitude mean ± ± SD; max velocity mean ± SD; duration mean ± SD.

RESULTS

1. Intraoperative Recordings

The purpose of this part is to demonstrate an increase in the precision and automaticity, if in addition to the STN border found by the neurologist-neurosurgeon team, one uses supplementary signals: power spectrum of the background activity – MUA and/or power spectra of LFP (p_LFP). We have already demonstrated good correlations between MUA and IOM (intra-OP monitoring – the standard procedure) using the statistical approach. Here we have demonstrated the use data mining (RSES) and machine learning (ML) methods.

Spike Trains, Background Activity and Local Field Potentials

As we have described in the Methods section, in the UMass experiments we have compared STN border estimations by three different methods: 1) classical "golden standard" IOM (intra-operative monitoring); 2) MUA – an increase in the power spectrum in the high frequency background multi unit activity (HFBA) [7]; 3) p_LFP – an increase in the power spectrum of the local field potentials.

In Fig. 3 we have plotted the results of these three methods together on one graph. The gray area is related to the IOM found during surgery by the neurosurgeon-neurologist team. The continuous line represents the spline approximation of the HFBA power spectra – MUA (interrupted line curve). There is very good agreement between IOM and MUA. The third curve (interrupted line) represents the power spectra of the LFP with the STN borders estimation. This curve is not very exact but only in approximate agreement to other measures. A question arises if the measure of the LFP can help in STN border estimation, even if it is not very precise measure.

As we have demonstrated before [7], the mean difference between IOM (intra-OP monitoring) and MUA (multi-unit power spectra background activity) of the dorsal/ventral border was 0.31 ± 0.84/0.44 ± 0.47 mm. The correlation between the dorsal border/ventral border positions obtained by IOM and MUA was 0.79, $p < 0.0001$/0.91, $p < 0.0001$ [7]. However, we did not ask the question: how well could we predict the STN borders on the basis of MUA in individual patients? For example for Pat 10 L, we have got good agreement between IOM and MUA for the STN dorsal border and a large difference between both methods in the STN ventral border estimation on the left side. What difference should we expect in both methods agreement for the right side for which we have only IOM measurements?

We did not respond to the above questions using data mining RS theory, as in this case the question was too demanding for our limited number of measurements. However, we were more successful in responding to a similar question in another series of the intra-OP recordings [16,17,18,19] performed by the team of Dr. Mandat [10]. All the recordings were divided into two groups: related to spike trains and to background activity. The spikes were detected on the basis of their amplitude and sorted into different shapes. In the first group, the main properties (attributes) were: 1) average number of recorded spikes; 2) spike burst ratio (percentage of intra-spike intervals shorter than 33 ms). However, these attributes may give both false positive (highly active non STN neurons) and false negative (less active STN parts) results. In the second group, the main attributes were: 1) relative amplitude of the background activity (80^{th} percentile – denoted as PRC_{80}; 2) Root Mean Square (RMS) calculated for the recorded signal; 3) LFB (low frequency background power) for frequencies below 500 Hz; 4) HFB (high frequency background power) for frequencies 500–3000 Hz [16,17]. Additional attributes obtained by moving the average of the primary attributes [18] were also used. Ciecierski et al. [19] have used in addition to RSES also the Weka Random Forest classifier. Both methods in the 10-folds cross validation gave excellent discrimination between recordings made within the STN and outside of it. It was based on the comparison of neurologist expertise with the results of classifications. The sensitivity was about 93% and specificity about 99% [19]. The second coefficient is even more important as it minimizes the probability of labeling a non-STN region as STN. These results are very promising as they were based on not only very large numbers of recordings (over 16000) but also on many different attributes describing signals recorded at different depths. As the system is already used in on-line surgeries, it may lead to increasing the speed and precision of DBS surgery.

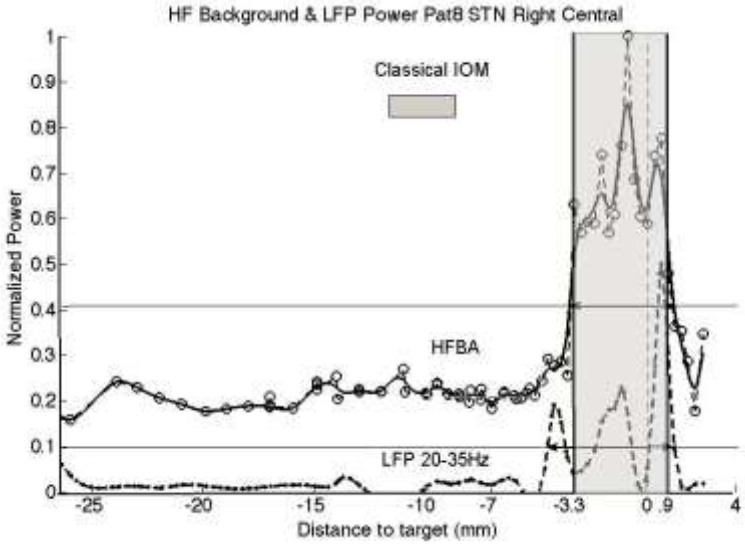

Fig. 3. Comparison of MUA – multi unit HFBA (high frequency background activity) and LFP (local field potentials) power spectra with STN borders determined by classical IOP (intra-OP monitoring – gray area).
Ryc. 3. Porównanie MUA /HFBA (aktywność tła o wysokiej częstotliwości) i LFP (lokalne potencjały polowe) widma mocy z granic określonych przez STN klasycznej IOP (monitoring wewnątrz PO – szara strefa).

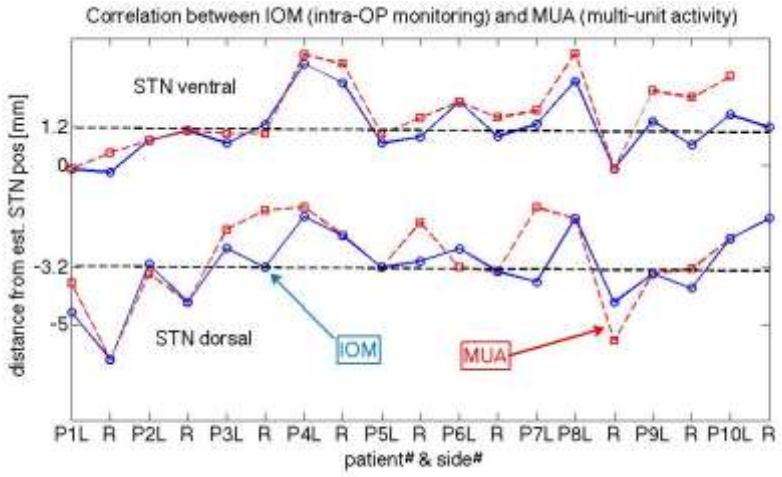

Fig. 4. Comparison of STN dorsal and ventral border determination by standard intra-op monitoring (IOM) and multi unit background activity (MUA).
Ryc. 4. Porównanie grzbietowej i brzusznej granicy STN wyznaczonej przez standardowy monitoring (IOM) i aktywności tła (MUA).

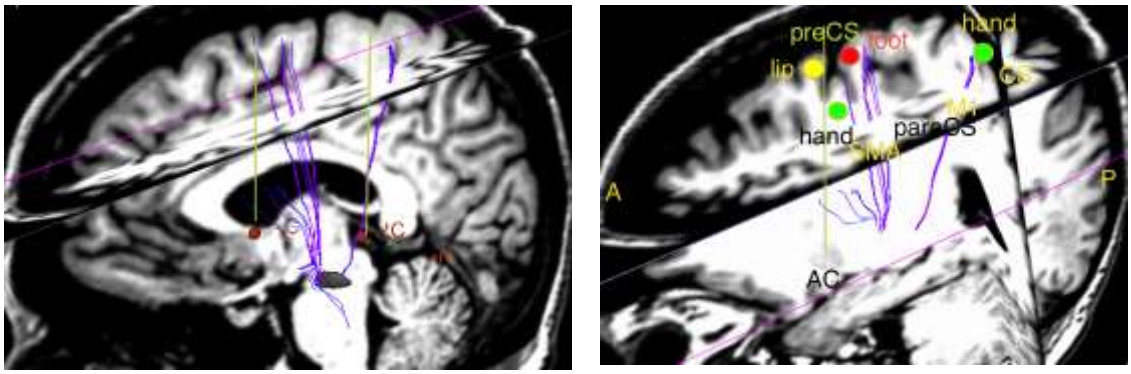

Fig. 5. Two MRI images of same area of Pat#5 with different views. They are mainly sagittal also with axial and coronary MRI images of left hemisphere with marked neural pathways between contact #1 left DBS electrode and different cortical areas. A, P – anterior, posterior; AC, PC – anterior, posterior commiserate that determine area of interest: between preCS and CS; SMA – supplementary motor area; M1 – primary motor area; CS – central sulcus; paraCS – para-central sulcus; preCS – precentral sulcus; lip, hand, foot – somatotopic areas representing lip, hand, foot. The STN is visible in the left image.
Ryc. 5. Dwa obrazy MRI tego samego obszaru. Obrazowanie w płaszczyźnie strzałkowej również z osiowymi i wieńcowymi obrazami MRI lewej półkuli z oznakowanymi szlakami nerwowymi między elektrodą DBS i różnymi obszarami kory. STN widoczny po lewej stronie obrazu.

2. Improving DBS parameters in relationship to electrode contact positions

In this session, we present the MRIs of one PD patient with implanted DBS electrodes. Fig. 5 shows the sagittal images of pat#5 left hemishere with marked tracts generated from contact #1 of the DBS electrode. The STN tracts have endings in the primary (M1) and supplementary motor areas (SMA). In M1 they come near the area representing the "hand", in SMA, posterior to the precentral sulcus near the area representing the "foot".
The results of patient #5 pre-Op neurological examinations were: dystonic cramps in feet, freezing gait, falls, mild depression, rigidity, minor tremors in legs and hands, cramping in left foot, later in both feet. The effects of DBS contact #1 stimulations on the left side were: improved dexterity and limb tone was normal in the right upper extremities, restless leg symptoms no longer present. Fig. 5 supports such findings, as there are tract endings near the foot and hand areas in the left hemisphere. Our question was if on the basis of our anatomical tracts we can predict which contact and what the amplitude of stimulation should be in order to improve particular symptoms.
In order to test this possibility, we divided our data of 20 measurements into 4 random groups.
We used 3 groups together for the training and tested the fourth group by applying rules generalised from the training sets. In the next step, we changed the

tested group for one training group and checked our predictions again. We performed testing of all the groups by the cross validation method. We obtained a total accuracy of 75–80%, which gives good predictions for such a small dataset [11]. By using this method we may increase the effectiveness of choosing optimal stimulating parameters as well as try to test parameters that may improve particular symptoms.

3. Gait measurements and classifications

In this simple example we concentrate only on PD pathologies of normal gait, and present several different approaches to compute important features of gait abnormalities. This is a continuation of our previous experimental results concerning the examination of Parkinson's disease (PD) involving a bilateral subthalamic nucleus stimulation (DBS) patient in the MoCap laboratory. At first, in the statistical approach we calculate the mean changes of gait as the effects of medication and DBS (deep brain stimulation of STN). In the second approach, we present the gait parameter changes in the phase plots that demonstrate different dynamics in different patients. In the third part, we apply the data mining approach related to application of the Rough Set Theory in order to generate decision rules for all our patients and all the experiments. We have tested these rules by comparing training and test sets using machine learning methods.

There have been many studies where the diagnosis of human gait abnormalities is measured in a more precise way than the result of the UPDRS test. In our previous work, we computed indexes for neurological gait abnormalities for PD patients with DBS [15]. We found a strong influence of medication and DBS on the decomposition index of the knee and hip, and hip and ankle. Therefore in this section we have concentrated on analysing the dynamics of hip movements of the gait [20].

However, the present approach is different from our previous work as now we intend to use not only the statistical analysis of certain indexes, but also the **data mining approach** based on the Rough Set Theory. This new approach not only summarizes the actual measurements but also gives some strong predictions that might be better than standard indexes, which can also predict the effects of different therapies for PD patients. As the effects of medications and DBS are very different in different patients, making predictions is a very difficult task and we present here only the preliminary data.

The mean for all patients' *UPDRS III* improved with sessions, **S1**: 53± 4 (SE), **S2**: 35 ± 6, **S3**: 22 ± 3.5, **S4**: 18 ± 3. The mean duration of three consecutive steps were similar between sessions: **S1**: 3.9 ± 0.2 s (SE), **S2**: 3.6 ± 1.6 s, **S3**: 3.6 ± 1.4 s, **S4**: 3.5 ± 1.2 s. These values are similar to the slow walk of a healthy person. In this study, we have limited our analysis to x-direction changes in the hip angles for the left and right legs during three consecutive steady steps of all PD patients [20].

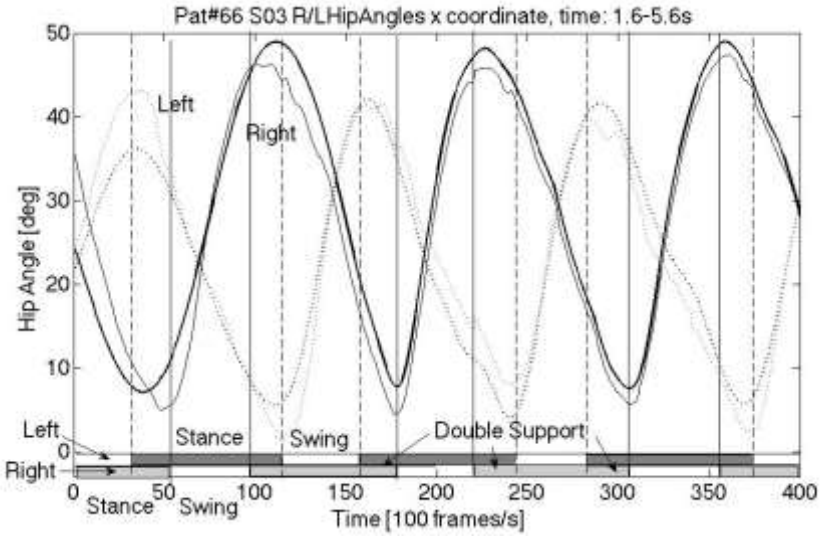

Fig. 6. Hip Euler angle during walking for right and left sides. In addition to hip angle changes (thin line) their smoothed changes (thick lines) by emd (elementary mode decomposition) were plotted together. In lower part, two phases of gait were marked. Velocities in both gait phases are plotted below.
Ryc. 6. Zmiany biodrowego kąta Eulera w trakcie chodu dla prawej i lewej strony.

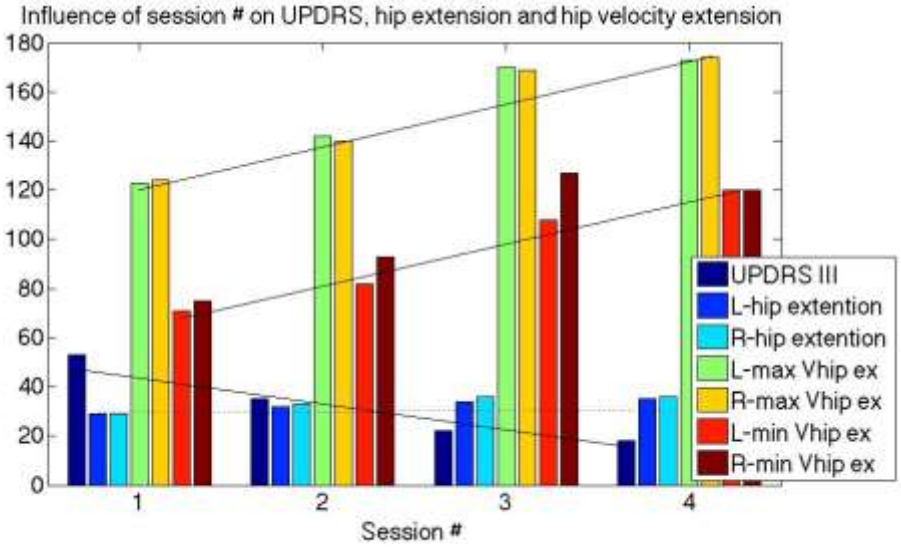

Fig. 7. Parallel changes in UPDRS III and left- and right-hip x-angle extensions, and left-, right maximum velocities during swing and stance (marked as max/min velocity) phases as effects of medication and STN stimulation (sessions 1 to 4). Straight lines approximate UPDRS decrease with session number and velocity increase proportionally to session number. Hip amplitude stays approximately independent of session number (interrupted line).
Ryc. 7. Równoległe zmiany w UPDRS III lewego i prawego stawu biodrowego jako skutki działania leków i stymulacji STN (1 do 4).

The means of the *maximum x-direction hip angles extension* (swing phase) for the left (L) and right (R) sides were symmetric and improved non-significantly between sessions, **S1**: L: 29 ± 3 deg (SE), R: 29 ± ± 3 deg (SE), **S2**: L: 32 ± 3 deg, R: 33 ± 3 deg, **S3**: L: 34 ± 3 deg, R: 36 ± 3 deg, **S4**: 35 ± 4 deg R: 36 ± ± 3 deg. We also found non-significant improvements for the *x direction hip angle flexion* (stand phase) between sessions. However, we have observed more significant improvements in the *maximum velocity of the x-direction hip angles extension* (velocity in the swing phase): **S1**: L: 123 ± 8.5 deg/s, R: 124 ± ± 9.5 deg/s; **S2**: L: 142 ± 6 deg/s, R: 140 ± 8.4 deg/s; **S3**: L: 170 ± 6.5 deg/s, R: 169 ± 9 deg/s; **S4**: L: 173 ± ± 6 deg/s, R: 174 ± 9 deg/s; and *hip angle flexion speed* (velocity in the stand phase): **S1**: L: 71 ± ± 8.5 deg/s, R: 75 ± 5 deg/s; **S2**: L: 82 ± 6 deg/s, R: 93 ± 6 deg/s; **S3**: L: 108 ± 7 deg/s, R: 127 ± 8 deg/s; **S4**: L: 120 ± 9 deg/s, R: 120 ± 9 deg/s (Fig. 7) [20].

Notice that the most significant increase in velocities was between sessions S1 and S3, so it is an effect of medication. On the basis of mean values for all our patients, we can say that medication as well as DBS improve patients' UPDRS and (hip) movement velocities. L-DOPA as well as DBS are well-established methods so one would expect such results. However, **individual patients are very different** and even in our small patient population we have observed significant variability of the medication and stimulation effects. Therefore, we would like to learn if we can group the effects of medication and DBS therapies of individual patients into several categories.

In addition to statistical analysis, we have tried two different methods; the first one was related to **dynamical system analysis** and the second to the **machine learning** approach. In our first method, we compared the phase plots for individual patients in four sessions S1 to S4. We plotted the movement trajectories in the phase space as changes of the right hip x-angles as a function of the left hip angle changes during three steps of stable walking. We found different types of attractor changes as the effect of medication and stimulations, as demonstrated in the following figures.

In summary, stimulation and medication generally increase the amplitude and shift trajectories related to PD patient walking activity. It is not mainly related to the patient's gait speed as the mean gait durations were similar in all the sessions. These plots might give basis for the dynamical model of gait in different sessions but as demonstrated, in different patients changes of the particular trajectory are difficult to predict as they are effects of the system complexity and basal ganglia regulatory numerous loops interactions.

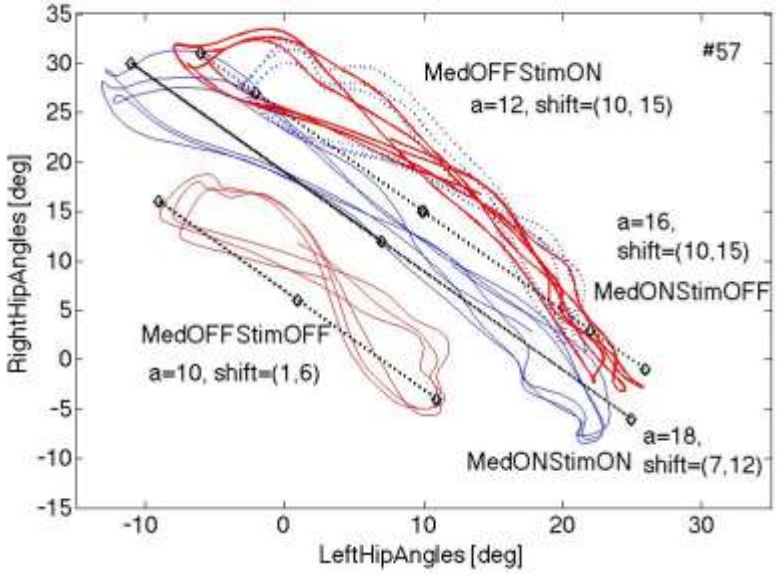

Fig. 8. Phase plots of right against left x direction hip angles during walking in one patient. Left: stimulation and medication extend trajectories and shift them up and right. Right: medication extends trajectories and shifts them down.
Ryc. 8. Wykresy fazowe z lewej na prawą w kierunku bioder i kątami podczas chodu u jednego pacjenta. Po lewej: stymulacja i leki wydłużają trojektorie i przesuwają je w górę i na prawo. Po prawej: lek wydłuża trajektorie i przesuwa je w dół.

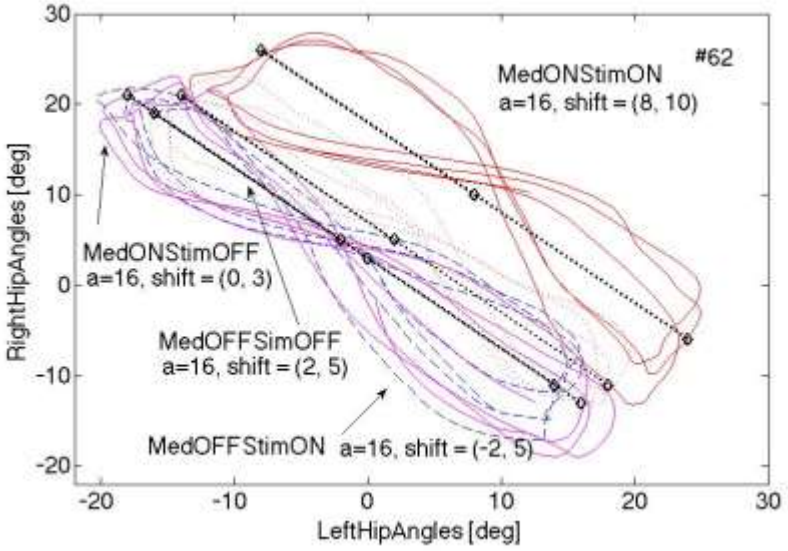

Fig. 9. Phase plots of right against left x hip angles during walking in one patient. Left: v. small effects of stimulation alone, medication also has small effects: extends trajectories and shifts them up. Right: v. small differences between S1, S2 and S3 in S4 (MedON, StimON) shift to right.
Ryc. 9. Wykresy fazowe – prawy i lewy kąt biodrowy podczas chodzenia u jednego pacjenta. Po lewej: małe efekty stymulacji, lek również wywiera słabe efekty: rozciąga trajektorie i przesuwa je. Po prawej: małe różnice między S1, S2 i S3 w S4 (Medon, Stimon) przesunięcia w prawo.

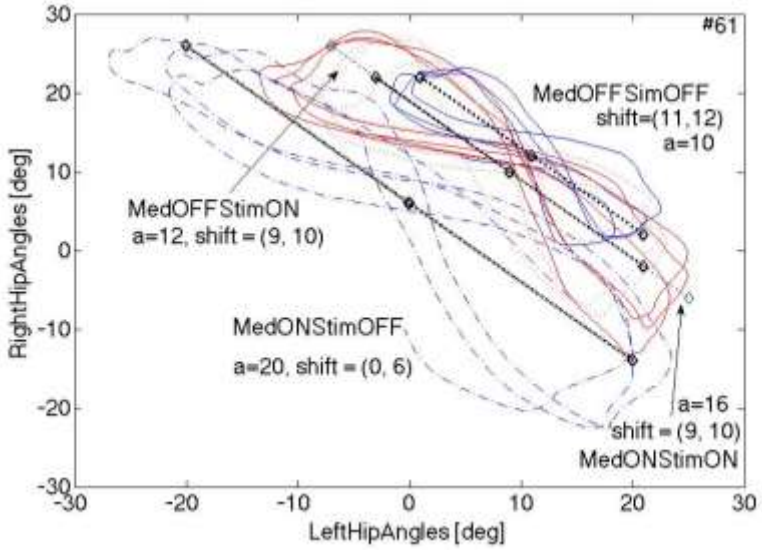

Fig. 10. Phase plots of right against left x hip angles during walking in one patient. Left, additive effects: both stimulation and medication alone shift trajectories up with extension, both together have stronger effects. Right, when medication OFF, stimulation extends amplitude of trajectories, medication increases their amplitude even more and shifts down, when MedON and StimON trajectories shift again up.
Ryc. 10. Wykresy fazowe kątów biodrowych podczas chodzenia u jednego pacjenta. Po lewej stronie działanie addytywne: zarówno stymulacja, jak i same leki powodują przesunięcia trajektorii z rozszerzeniem, razem mają silniejsze działanie. Po prawej stronie, leki OFF, stymulacja zmniejsza amplitudę trajektorii.

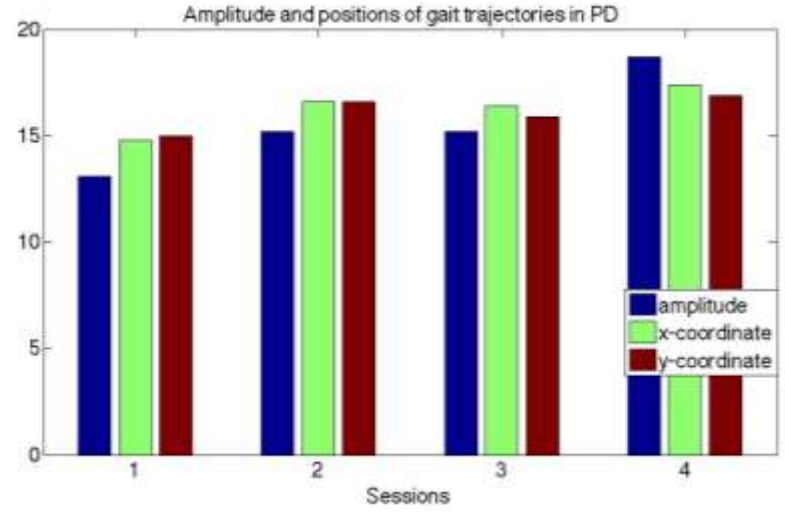

Fig. 11. Parallel changes in left-right angle trajectories amplitude, x- and y- coordinates during walking as effects of medication and STN stimulation.
Ryc. 11. Równoległe zmiany lewa-prawa trajektorii, kąt amplitudy, współrzędne X i Y podczas spaceru jako działanie leków i stymulacji STN.

4. Data Mining – Rough Set System Approach

As described above, we have used RSES 2.2 (Rough System Exploration Program) [21] in order to find regularities in our data. At first, our data was placed in the decision table as originally proposed by Pawlak [5]. In each row of the decision table there are the following condition attributes: P# – patient#, S# – Session#, t – time, mxaL/mxaR/mnaL/mnaR – max/min Left/Right hip x-direction angles, mxVaL/mxVaR/ mnVaL/mnVaR – max/min Left/Right hip x-direction velocity, and UPDRS III as measured by the neurologist in the last column. There are data from two out of 12 patients in the table below:

Table I. Extract from information table
Tabela I. Część tabeli informacyjnej

P#	S#	time	mxaL	mxaR	mnaR	mnaL	mxVaL	mxVaR	mnVaL	mnVaR	UPDRS
59	1	455	29.1	32.3	-0.04	-0.86	0.91	0.91	-0.60	-0.66	30
59	2	350	34.7	35.6	-1.25	-9.07	1.77	1.77	-0.99	-1.31	20
59	4	350	31.9	35.9	-3.29	-8.19	1.67	1.67	-1.00	-1.24	6
61	1	305	20.7	22.9	-0.92	1.35	1.28	1.28	-0.61	-0.69	60
61	2	440	22.4	25.9	-8.05	-5.87	1.31	1.31	-0.53	-0.68	40
61	3	410	21.1	25.1	-23.4	-21.77	1.98	1.98	-1.05	-1.30	21
61	4	400	24.4	27.2	-12.0	-10.58	1.56	1.56	-0.93	-0.82	31

The last column represents a decision attribute, then we can write for each row a decision rule as follows:

('Pat' = 59)&('Sess' = 1)&('time' = 455)& ('mxaL' = 29.1)&('mxaR' = 32.3)&… = > ('UPDRS' = 30) (1)

We read this rule as follows : if for patient #59 and session S1 and the time of his/her three steps was 4.55 s and max left hip x-direction angle equals 29.1 deg and max right hip x-direction angle equals 32.3 deg and … then his/her UPDRS III for these conditions was 30.

Therefore we have obtained 46 decision rules directly from our measurements as two from our 12 patients did not have all four sessions (e.g. pat#59). The main purpose of our analysis is to reduce these rules and to find regularities in our data. There are many possible steps as described in [21], below we will give some examples.

At first, we would like to make the rules shorter and find that they apply to more than one case, e.g.:

('Pat' = 60) = > ('UPDRS' = 9[2]) 2 (2)

('mnVaL' = -0.6756) = > ('UPDRS' = 32[2]) 2 (3)

it reads that Pat# 60 obtained UPDRS = 9 in two sessions (eq. 2) and that the minimum velocity of the left hip equals -0.6756 (- is related to the direction of gait) was related to UPDRS = 32 in two cases (eq.3). In order to make the rules more effective, RSES can find optimal linear combinations of different attributes like:

*'mxVaL'*0.594+'mxVaR'*(-0.804)* (4)

*'mx_aL'*0.046+'mn_aL'*(-0.587)+'mn_aR'*0.807* (5)

and these linear combinations may be added as additional attributes. Furthermore we can use the discretization procedure [21] that divides attribute values into non-overlapping parts:

('Pat' = "(58.5,Inf)")&('Sess' = "(2.5,3.5)"|"(3.5,Inf)")&('mnVaL' = "(-0.9803,Inf)") = > ('UPDRS' = 32[3]) 3 (6)

This reads that for patients that have numbers above 58.5 and in sessions S3, S4 the minimum hip velocity was -0.9803 or above, then the UPDRS equals 32 in three cases (eq. 6).

As we have demonstrated above, the rules determining the possible UPDRS are important but from the patient and doctor points of view, the first message should be whether the current therapy (medication and/or DBS) is effective. In order to find it, we need to correlate our measurements with the session number that is related to the specific procedure. In this case, the session number will become the decision attribute, in other words we change the columns of the decision table (tab. I) in such way that the session numbers are moved to the last column and become decision attributes. Notice that the session numbers may simulate symptom development in time (in the reverse direction S4, S3, S2, S1). In this case, we can obtain the following more general rules e.g.:

('UPDRS' = 52|53|43|56|87|45|58|30|60) = > ('Sess' = 1[11]) 11 (7)

('UPDRS' = 23|13|43|22|39|28|24|81|48|42) = > ('Sess' = 2[11]) 11 (8)

('time' = 440|305|280|365|310) = > ('Sess' = 2[6]) 6 (9)

this means that session S1 (MedOFFStimOFF) is related to a high UPDRS in 11 cases (eq. 7), in session S2 (MedOFFStimON) the UPDRS values are generally smaller in 11 patients (eq. 8) and in this session (S2) the duration of three steps is between 2.8 and 4.4 s in 6 cases (eq. 9). We can also for example find rules in which the duration of three steps are similar as in (eq. 10):

('time' = 350)&('Pat' = 56|57|62|59) = > ('Sess' = 4[4]) 4 (10)

In the next two examples, we will demonstrate how we can use general rules to predict the session number (or symptom development in time) or UPDRS values in – a group of patients that do not have these measurements that may mimic a group of new patients. We will use the machine learning algorithms (ML). The main purpose of the ML approach is to demonstrate that the proposed rules are universal enough to predict

the results from new patients on the basis of already measured patients (*test-and-train scenario* [6,21]). In order to perform a such test, we divided our data set into two parts: one 60% of our data was the training set, and another 40% was the set that had been tested. We removed the decision attributes from the test set and compared them with the attribute values obtained from our rules. We used several different algorithms in order to find rules from the training set. The exhaustive algorithm [21] gave the best results described in the confusion matrix below:

Table II. Confusion matrix for different session numbers (S1–S4)
Tabela II. Macierz błędów dla sesji S1-S4

		Predicted				
		2	**3**	**4**	**1**	**ACC**
	2	2	0	0	1	**0.66**
Actual	**3**	1	0	1	2	**0.0**
	4	1	3	1	0	**0.2**
	1	0	1	1	2	**0.5**
	TPR	**0.5**	**0.0**	**0.33**	**0.4**	

TPR: True positive rates for decision classes, ACC: Accuracy for decision classes.

Coverage for decision classes: 0.75, 1.0, 1.0, 0.66 and global coverage = 0.8421, and global accuracy = = 0.3125. The best prediction was for session 2 with an accuracy of 0.66 (tab. II), and session 1 with accuracy of 0.5, the other session did not produce good predictions. The global accuracy over 31% was not very good. It is probably related to the small set of data. It means that we probably need to use more rules, for example, combinations of many attributes or/and expand the number of measured attributes for our analysis.

However, the problem with this approach is that its results depend on which part of our measurements was taken as training and which part was tested. In order to test in an exhaustive manner or all the different possibilities, we divided our experimental random set into 9 subsets. In the next nine steps, we removed the decision attributes from one set and all the others used for training and prediction of the removed attributes from the test set. After 9 tests for all the parts, the results were averaged. We performed these tests for UPDRS as the decision attribute. Before all the tests the UPDRS values were divided into 6 classes, and the predictions were compared with the actual results for each class as summarized below in the confusion matrix:

Table III. Confusion matrix for UPDRS as decision attribute
Tabela III. Macierz błędów dla atrybutu decyzyjnego UPDRS

		PREDICTED					
		50,69.5	**-Inf,29.5**	**42.5,50**	**34,42.5**	**69.5,Inf**	**29.5, 34**
A	**50, 69.5**	0.67	0.0	0.0	0.0	0.0	0.0
	-Inf, 29.5	0.0	1.67	0.0	0.11	0.11	0.0
C	**42.5,50**	0.0	0.0	0.11	0.0	0.0	0.0
T	**34,42.5**	0.0	0.11	0.0	0.0	0.0	0.0
U	**69.5, Inf**	0.0	0.11	0.0	0.0	0.0	0.0
A	**29.5, 34**	0.0	0.0	0.0	0.0	0.0	0.22
L	TPR	**0.44**	**0.71**	**0.11**	**0.0**	**0.0**	**0.22**

TPR: True positive rates for decision classes, **ACC:** Accuracy for decision classes: 0.44, 0.72, 0.11, 0, 0, 0.22. Coverage for decision classes: 0.44, 0.60, 0.11, 0.11, 0.11, 0.17 and global coverage = 0.6, and **global accuracy = 0.917**. UPDRS decision classes: (50, 69.5), (- Inf, 29.5), (42.5, 50), (34, 42.5), (69.5, Inf), (29.5, 34).

If we look at the global accuracy, it is about 92% so we have good agreement between the predicted and actual UPDRS values. The reason is that over half of all the UPDRS values are below 29.5 and they were very well predicted, as well as the UPDRS values between 50 and 69.5, (42.5,50), and (29.5,34). It is good a result even though the global coverage = 0.6 is not great.

5. Reflexive saccades measurements and classifications

The patients' mean age was 51.1 ± 10.2 (SD) years, mean disease duration was 11.3 ± 3.2 years, mean UPDRS: S1: 66.6 ± 13.8 S2: 30.0 ± 16.3; S3: 58.1 ± ± 13.5; S4: 22.3 ± 13.6; mean UPDRS III: S1: 42.7 ± ± 11.3 S2: 17.8 ± 10.6; S3: 34.1 ± 10.8; S4: 10.9 ± ± 8.3; mean RS latencies: S1: 291.2 ± 93.1 ms, S2: 199.6 ± 39.5 ms, S3: 232.9 ± 82.7 ms; S4: 183.2 ± 30 ms. The differences between latencies: S1–S2, and S1–S4 were statistically significant (t-test $p < 0.01$), S1–S3 – – not stat. sig., similar to differences between UPDRS/UPDRS III: S1–S2, and S1–S4 were stat. sig ($t < 0.001$) and S1–S3 – not stat. sig. [22]. Other RS parameters did not change significantly with session number.

The full table has 11 attributes and 32 objects (measurements). In each row of the decision table there are the following condition attributes: P# – patient#, age – – patient's age, sex – patient's sex: 0 – female, 1 – male, t_dur – duration of the disease, S# – Session#, UPDRS – total UPDRS, HYsc – Hoehn and Yahr scale all measured by the neurologist and saccades measurements: SccDur – saccade duration; SccLat – saccade

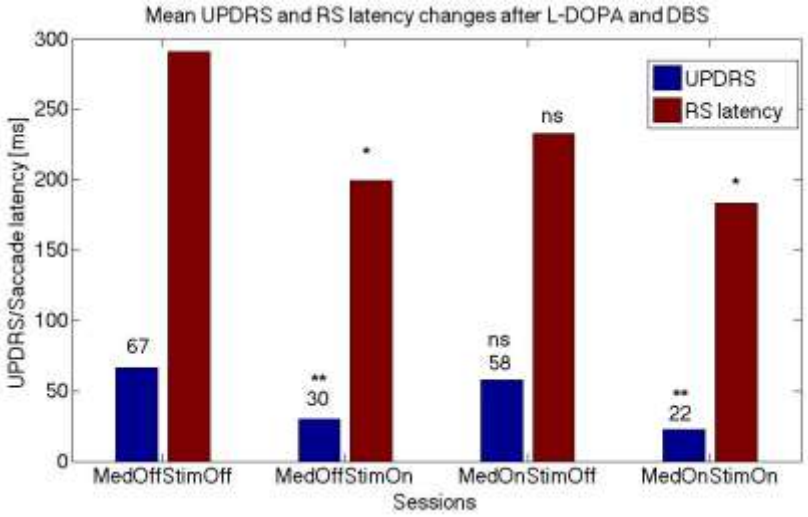

Fig. 11. Parallel changes in UPDRS and reflexive saccades latencies as effects of medication and STN stimulation. Changes between control and Med*StimOn were significantly different for UPDRS $p < 0.001$ (**), RS $p < 0.01$ (*).
Ryc. 11. Równoległe zmiany w UPDRS i opóźnienia w odruchowych sakadach jako skutek działania leków i stymulacji STN. Różnice między kontrolą i Med*Stimon były znaczące dla UPDRS ($p < 0{,}001$), RS ** $p < 0{,}01$ (*).

Table IV. Extract from information table
Tabela IV. Część tabeli informacyjnej

P#	age	sex	t_dur	S#	UPDRS	HYsc	SccDur	SccLat	SccAmp	SccVel
28	54	1	8	1	58	2.0	43	402	12	566.9
28	54	1	8	2	40	1.0	46	297	11	474.5
28	54	1	8	2	40	1.0	49	227	10	431.2
28	54	1	8	4	16	1.0	47	198	9	376.2
38	56	0	11	1	49	2.5	42	285	14	675.2
38	56	0	11	2	22	1.5	48	217	12	509.7
38	56	0	11	3	37	2.5	43	380	14	638.9
38	56	0	11	4	12	1.5	45	187	10	482.6

latency; SccAmp – saccade amplitude, and SccVel – – saccade velocity. In the next step, we performed reduction of the attributes (see reduct in the Method section) to minimumize the number of attributes describing our results. In the following step, we performed table discretization which means that single values of measurements were replaced by their range (as describe in the Method section: cut sets). As a result we have obtained a decision table (Tab. V – see below).

In the first column is the patient's number, in the second: patient's age divided into patients below (Pat#28) or above (Pat#38) 55 years of age; disease duration and Hohn and Yahr scale were not important (stars), session number is the same; and other saccades parameters were also divided into ranges. It is interesting how the UPDRS values were divided into different ranges: above 55, 22.5 to 55, 14 to 22.5, and below 14 (the last column). On the basis of the decision table we can write the following rule:

('Pat' = 28)&('age' = "(-Inf,55.0)")&('Sess' = 1)&
('SccDur' = "(-Inf,45.5)")&('SccLat' = "(260.0,Inf)")
&(' SccAmp') = "(10.5,Inf)") = >
('UPDRS' = "(55.0,Inf)") (11)

We read this as the formulas above (eqs. 1–10), and each row of the table (tab. V) can be written in the form of this equation (eq. 11). These equations are parts of the data mining system based on the Rough Set Theory [5]. On this basis we have found more general rules describing our measurements in a similar way as mentioned above (eqs. 6–9). In the next step, we tested our rule using the machine-learning concept. We randomly divided our data into 4 groups, we took 3 groups as a training set and the fourth was tested. By changing groups belonging to the training and test sets, we removed the effect of accidental division. The results of each test were averaged. It is called the 4-fold cross-validation that gave us the results in the confusion matrix (tab. VI). As a machine-learning algorithm we used the decomposition tree (see Methods).

We have performed several tests trying to predict UPDRS values on the basis of measuring saccades properties. As the changes in UPDRS and saccades latencies were similar when the session number changed (Fig. 11), we tried to predict individual UPDRS values only from the RS latencies, but we did not get good results. Nevertheless, when, the patient´s age, RS: latency, amplitude, and duration were added to the session number, the global accuracy in UPRDS prediction was 70% (ML: decomposition tree, cross-validation-method). This is a good result for such a small population showing the power of data mining and machine learning methods in neurology.

Table V. Extract from decision discretized-table
Tabela V. Część zdyskretyzowanej tabeli decyzyjnej

P#	age	t_dur	S#	HYsc	SccDur	SccLat	SccAmp	UPDRS
28	"(-Inf,55.0)"	*	1	*	"(-Inf,45.5)"	"(260.0,Inf)"	"(10.5,Inf)"	"(55.0 Inf)"
28	" (-Inf,55.0)"	*	2	*	"(45.5,Inf)"	"(260.0,Inf)"	"(10.5,Inf)"	"(22.5,55.0)"
28	"(-Inf,55.0)"	*	2	*	"(45.5,Inf)"	"(-Inf,260.0)"	"(-Inf,10.5)"	"(22.5,55.0)"
28	"(-Inf,55.0)"	*	4	*	"(45.5,Inf)"	"(-Inf,260.0)"	"(-Inf,10.5)"	"(14.0,22.5)"
38	"(55.0,Inf)"	*	1	*	"(-Inf,45.5)"	"(260.0,Inf)"	"(10.5,Inf)"	"(22.5,55.0)"
38	"(55.0,Inf)"	*	2	*	"(45.5,Inf)"	"(-Inf,260.0)"	"(10.5,Inf)"	"(14.0,22.5)"
38	"(55.0,Inf)"	*	3	*	"(-Inf,45.5)"	"(260.0,Inf)"	"(10.5,Inf)"	"(22.5,55.0)"
38	"(55.0,Inf)"	*	4	*	"(-Inf,45.5)"	"(-Inf,260.0)"	"(-Inf,10.5)"	"(-Inf,14.0)"

Table VI. Confusion matrix for different session numbers (S1–S4)
Tabela VI. Macierz błędów dla różnych sesji S1–S4

		Predicted				
		55.0,Inf	**22.5,55.0**	**-Inf,14.0**	**14.0,22.5**	**ACC**
Actual	**55.0,Inf**	0.6	0.3	0.2	0.0	**0.33**
	22.5,55.0	0.1	1.3	0.0	0.0	**0.8**
	-Inf,14.0	0.0	0.1	0.2	0.0	**0.2**
	14.0,22.5	0.0	0.2	0.0	0.0	**0.0**
	TPR	**0.45**	**0.6**	**0.2**	**0.0**	

TPR: True positive rates for the decision classes, ACC: Accuracy for the decision classes, the global coverage was 1.0, the global accuracy was 0.7, the coverage for the decision classes: 0.7, 0.9, 0.3, 0.2.

DISCUSSION

We have given several examples related to comparison of the classical measures performed by most neurologists and our new approach. The main difference between these measures is their precision and objectivity. Our approach is doctor-independent and can be performed automatically. In the near future it may lead to replacing hospital-oriented with home-oriented medicine. It will give new options to patients such as to measure their symptoms at home and to send their results to the hospital for consultation with a neurologist. Such methods will be faster, more precise and can help to obtain more frequent measurements. In consequence, they may help not only to determine patients' symptoms more objectively, but also to follow disease progression in short periods of time that it is not possible nowadays with the limited means and time of neurologists. If we obtain such information, it may lead to slowing down of disease progression. Slowing down disease progression remains the single most important unrealized need in PD treatment. Even with a large number of clinical trials, we are still unable to produce conclusive results. There are multiple reasons for such failures. First of all, there are the shortcomings of current disease models in target validation and potentials tests, difficulties in choosing clinical endpoints, as well as finding sensitive biomarkers in disease progression. One problem is that the disease starts long before the observed motor symptoms and individual pathological mechanisms have a large spectrum. One of the purposes of this work is to try **to extract knowledge from symptoms** in order to model possible mechanisms of disease progression as exemplified in Fig. 1.

CONCLUSIONS

Data mining and ML approaches are more precise and powerful than popular statistical methods. On the basis of finding modus ponens rules in experimental sets, we can apply them to predict disease progression not only in a particular patient, but also in new patients in order find possible ways to slow down the development of their symptoms.

ACKNOWLEDGEMENT

This work was partly supported by projects NN 518289240 and DEC-2011/03/B/ST6/03816 from the Polish National Science Centre.

REFERENCES

1. Przybyszewski A. The Neurophysiological Bases of Cognitive Computation Using Rough Set Theory. In: Transactions on Rough Sets IX. Eds. J.F. Peters et al. Springer Verlag, Berlin–Heidelberg 2008, LNCS 2008; 5390, 287–317.
2. Przybyszewski A. Logic in Visual Brain: Compute to Recognize Similarities. Formalized Anatomical and Neurophysiological Bases of Cognition. Review of Psychology Frontier 2012; 1: 20–32.
3. Przybyszewski A. Logical rules of visual brain: From anatomy through neurophysiology to cognition. Cognitive Systems Research 2010; 11: 53–66.
4. Sebok M., Erlacher A., Seiler S., Homann C.N. Non-motor features and motor complications in IPD: are UPDRS parts I nad IV relevant evaluation tools? European Neurology Meeting 15 October 2013. J. Neurol. Sci. 2013, 333, suppl. 1: e87.
5. Pawlak Z. Rough set. Theoretical aspects of reasoning about data. Kluwer Academic Publisher, Dordrecht 1991.
6. Bazan J., Szczuka M. RSES and RSESlib – a collection of tools for rough set computations. In: Rough Sets and Current Trends in Computing. Eds. W. Ziarko, Y. Yao. Springer Verlag, Berlin–Heidelberg 2001. LNAI vol. 2005, pp. 106–113.
7. Novak P., Przybyszewski A.W., Barborica A., Ravin P., Margolin L., Pilitsis, J. G. Localization of the subthalamic nucleus in Parkinson disease using multi unit activity. J. Neurol. Sci. 2011; 310: 44–49.
8. Kwiek S.J., Kłodowska-Duda G., Wojcikiewicz T. et al. Simultaneous targeting and stimulation of STN and VIM in tremor predominant PD patients. Pro's and cons. Acta Neurochir. 2006; 14(10): 36.
9. Kwiek S.J., Boczarska-Jedynak M., Świat M. et al. DBS for Parkinson's disease treatment. Experience and results interdisciplinary Silesian Centre for Parkinson's Disease Treatment in Katowice. Neurol. Neurochir. Pol. 2010; 44, supl. 1: S16-S17.
10. Pizzolato T. Mandat, T. Deep Brain Stimulation for Movement Disorders. Front. Integr. Neurosci. 2012; 6: 2. doi: 10.3389/fnint.2012.00002.
11. Talos I-F., Jakab M., Kikinis R., Shenton M.E. SPL-PNL Brain Atlas. SPL 2008.
12. Cauda F., Giuliano G., Federico D., Sergio D., Katiuscia S. Discovering the somato-topic organization of the motor areas of the medial wall using low-frequency BOLD fluctuations. Hum. Brain Mapp. 2011; 32: 1566–1579. doi: 10.1002/hbm.21132.
13. Mayer A.R., Zimbelman J.L., Watanabe Y., Rao S.M. Somatotopic organization of themedial wall of the cerebral hemispheres: a 3 Tesla fMRI study. Neuroreport 2001; 12, 3811–3814.
14. Szymanski A., Przybyszewski A.W. Rough Set Rules help to optimize parameters of Deep Brain Stimulation in Parkinson's Patients. In: Brain Informatics and Health. Eds. D. Ślęzak, A-H. Tan, J.F. Peters, L. Schwabe. LNAI 2014, vol. 8609, pp. 345–356.
15. Stawarz M., Kwiek S.J., Polanski A. et al. Algorithms for computing indexes of neurological gait abnormalities in patients after DBS surgery for Parkinson Disease based on motion capture data. Machine Graphics and Vision 2011; 20: 299–317.
16. Ciecierski K., Ras Z.W., Przybyszewski A.W. Foundations of recommender system for STN localization during DBS surgery in Parkinson's patients. Foundations of Intelligent Systems. ISMIS 2012 Symposium. Springer Verlag Berlin–Heidelberg 2012, LNAI vol. 7661, pp. 234–243.
17. Ciecierski, K., Ras Z.W., Przybyszewski A.W. Discrimination of the micro electrode recordings for STN localization during DBS surgery in Parkinson's patients. Flexible Query Answering Systems. FQAS 2013 Symposium. Springer Verlag Berlin–Heidelberg 2013, LNAI vol. 8132, pp. 328–339.
18. Ciecierski K., Ras Z.W., Przybyszewski A.W. Foundations of automatic system for intrasurgical localization of subthalamic nucleus in Parkinson patients. Web Intelligence and Agent Systems 2014; 12: 63–82.
19. Ciecierski K., Ras Z.W., Przybyszewski A.W. Intraoperative Decision Making with Rough Set Rules for STN DBS in Parkinson Disease. In: In: Brain Informatics and Health. Eds. D. Ślęzak, A-H. Tan, J.F. Peters, L. Schwabe. LNAI 2014, vol. 8609, pp. 323–334.
20. Przybyszewski A.W., Boczarska M., Kwiek S.J., Wojciechowski K. Rough Set Based Classifications of Parkinson's Patients Gaits. In: Intelligent Information and Database Systems. Eds. N.T. Nguyen, B. Attachoo, B. Trawiński K. Sombooviwat. ACIIDS 2014, Part II. Springer National Publishing. LNAI 2014; vol. 8398, pp. 525–534. 10.1007/978-3-319-05458--2_54.

21. Bazan J., Son Nguyen H., Trung Nguyen T., Skowron A., Stepaniuk J. Synthesis of decision rules for object classification. In: Incomplete Information: Rough Set Analysis. Eds. E. Orłowska. Physica Verlag, Heidelberg 1998, pp. 23–57.

22. Szlufik S., Dudkiewicz J., Przybyszewski A.W., Habela P., Koziorowski D. Reflexive saccadic eye movements latency as biomarker that correlates with UPDRS in Parkinson's disease patients. Mov. Dis. 2014; vol. 29, Suppl. Abstracts suplement.